An IoT-based Thermal Modelling of Dwelling Rooms to Enable Flexible Energy Management

Junlong Li, Chenghong Gu, Xiangyu Wei, Ignacio Hernando Gil, Yue Xiang

***Abstract*—The thermal model of dwellings is the basis for flexible energy management of smart homes, where heating load is a big part of demand. It can also be operated as virtual energy storage to enable flexibility. However, constrained by data measurements and learning methods, the accuracy of existing thermal models is unsatisfying due to time-varying disturbances.**

This paper, based on the edge computing system, develops a dark-grey box method for dwelling thermal modelling. This dark-grey box method has high accuracy for: i) containing a thermal model integrated with time-varying features, and ii) utilising both physical and machine-learning models to learn the thermal features of dwellings. The proposed modelling method is demonstrated on a real room, enabled by an Internet of Things (IoT) platform. Results illustrate its feasibility and accuracy, and also reveal the data-size dependency of different feature-learning methods, providing valuable insights in selecting appropriate feature-learning methods in practice. This work provides more accurate thermal modelling, thus enabling more efficient energy use and management and helping reduce energy bills.

***Index Terms*—Thermal model, machine learning, edge computing, data dependency.**

NOMENCLATURE

c	Specific thermal capacity, J/(kg·K)
H	Humidity, %
K	Thermal conductance, W/K
m	Mass, kg
N	Number of occupants inside a room
Q	Heat amount, J
R	Local solar radiation, W/m^2
T	Temperature, K
V	Volume, m^3
ρ	Density, kg/ m^3

Subscripts

a	Ambient air
d	Disturbances, including human behaviours, solar radiation, appliances, and so on
h	Heating radiator
o	Adjacent rooms
r	Room air
$r2a$	Subscripts formed in this way mean the thermal conductance from one to another, e.g., $r2a$ means a value from room air to ambient air
w	Walls connected to adjacent rooms
ε	Local area weather

I. INTRODUCTION

HEATING system in dwellings consumes a significant amount of energy in many countries. It accounted for 16.6% of total energy consumption in Europe, 2018 [1], and 17.4% in the UK, 2014 [2, 3]. To reduce carbon emissions in energy systems, electrifying heating systems to coordinate with renewable generations has become a crucial path worldwide [4]. Flexible energy management of heating systems is the key to coordinating heating loads with renewable generations in smart homes [5, 6]. To realise this, high-accuracy thermal models of dwellings are necessary for energy management systems (EMSs) to guarantee thermal comfort for customers [7]. Specifically, the temperature alternation caused by EMS operation should be estimated based on thermal models to control interior temperature within customers' comfort zone.

Thermal models are normally formed as a state-space function with more than ten parameters. However, these parameters, such as thermal capacity conductance, are difficult to directly obtain [8]. Therefore, these parameters need to be learned from measured data, named feature learning in this paper. It should be noted that the parameters of thermal models, such as air humidity and thermal disturbances from appliances and human beings, keep changing because of human behaviours and weather conditions. Thus, how to rationally combine these time-varying features into the thermal model and accurately learn them to improve the accuracy of the thermal model still needs to be solved. Besides, since temperature data could contain occupants' information, privacy protection is important in measuring and processing data. This leads to two crucial challenges: 1) Privately temperature measuring and data processing; 2) Accurate feature learning of thermal models integrated with time-varying features.

The first challenge can be facilitated by the emerging edge computing (EC) technology, which is suitable for distributed sensing systems [9]. EC refers to a platform that integrates network, computing, storage and application close to data sources [10, 11]. Temperature data collected by EC can be processed on the edge side without communication with other servers or routers, which physically avoids data leakage. Several EC-based temperature sensing systems for dwellings have been developed in previous works with different communication methods, such as Wi-Fi [12], Bluetooth [13]

Manuscript received July 24, 2022; revised Sep 23, 2022; accepted January 4, 2023. (Corresponding author: Chenghong Gu). Junlong Li and Chenghong Gu are with the Department of Electronic and Electrical Engineering, University of Bath, Bath, UK (jl3466@bath.ac.uk and cg277@bath.ac.uk).

Yue Xiang and Xiangyu Wei are with the College of Electrical Engineering, Sichuan University, Chengdu, China (xiang@scu.edu.cn and xiangyu_wei@163.com). Ignacio Hernando Gil (i.hernandogil@estia.fr) is with ESTIA Institute of Technology, Bordeaux, France.

and ZigBee [14]. Among these methods, ZigBee is more suitable for smart homes with fewer investment costs and higher stability [15]. Therefore, based on EC and ZigBee technologies, a data measurement and processing system is established in this paper to support thermal modelling.

As for the second challenge, feature learning is the key step of thermal modelling and is mainly realised in three ways: 1) White box, which assumes that all parameters of physical thermal models are well-known [16-18]; 2) Black box, where a thermal model is learned by machine learning methods without prior physical knowledge [19-21]; 3) Grey box, where machine learning is utilised to learn the parameters of physical thermal models [8, 22-24]. Since the white box is impractical due to the lack of specific detailed thermal parameters, and the black box is hard to interpret, the grey box is widely applied in modelling problems. Paper [8] develops a grey box to learn the thermal model based on Genetic Algorithms (GA). This method converges fast, but its results highly rely on the selection of the testing set. Papers [24] and [23] utilise Maximum Likelihood Estimation (MLE) to learn the thermal model. This method is easy to implement but difficult to provide accurate estimation for conditions that seldom appear in the training set. Paper [22] develops a thermal model based on the Trust region algorithm (TRA), GA and particle swarm optimization (PSO). However, this method, similar to the above methods, ignores time-varying features of thermal models, which keep changing with human behaviours and weather conditions.

This paper develops a dark-grey box to learn both constant and time-varying features of dwelling thermal models, enabled by a ZigBee-supported EC system. The dark-grey box contains two parts: a grey box to learn constant features and a black box to learn time-varying features so that both accuracy and interpretability are considered. This makes the method much closer to a black box, thus indicated as a dark-grey box. For the grey box, the constant feature is learned based on the physical thermal model of dwellings. Learning methods include traditional optimisation methods (PSO) and statistical methods (MLE and Kernel Density Estimation (KDE)). Clustering and classification strategies are also introduced to improve learning accuracy by dividing the dataset into different groups then learning features from them separately. Based on the results of the grey box, the time-varying features are learned by a deep Gated Recurrent Unit (GRU) neural network in the dark grey box. GRU network can capture time-sequence features with high efficiency [25], which can significantly improve learning accuracy compared with the grey box. This paper has the following contributions:

- Time-varying features are integrated into the thermal model to involve time-sequence variables, in which way the model's accuracy can be significantly improved.
- A dark-grey box is developed to learn dwellings' thermal models by integrating both grey and black boxes. The integrated black box improves the accuracy of grey-box feature learning. The grey-box basis makes it easy to interpret based on the physical model.
- A ZigBee-based edge computing platform is implemented for data acquisition and management, which provides stable communication with high privacy and is easy to deploy.

The rest of this paper is organised as follows: Section II shows the architecture of the EC-based system. Section III presents dwelling thermal modelling. The development of the dark-grey box with feature learning is presented in Section IV. The case study of the dark-grey box with related analysis is presented in Section V. The outlook and conclusion of this work are summarised in Sections VI and VII, respectively.

II. Architecture of ZigBee-Supported EC System

Feature learning methods and data measurement are enabled by an EC system based on ZigBee communication, as shown in Fig. 1. Temperatures from surroundings are collected by DHT-11 sensors connected to CC-2530 boards. DHT-11 is a widely used temperature-humidity sensor and CC2530 is a system-on-chip (SoC) solution for IEEE 802.15.4 ZigBee applications [26]. The temperature is measured from room air, ambient air, walls and radiators, as in Fig. 2. The perceptual layer consists of several sets of DHT-11 and CC2530. An additional CC2530 board is set as the central node to aggregate data from other CC-2530 boards via ZigBee communication and then sends them to EC nodes. A Raspberry Pi is utilised as the EC node, which communicates with the central node by serial communication.

Although this paper only focuses on the dwelling's thermal modelling, some functions like EMSs for heating systems can be further applied to the application layer. Based on an accurate thermal model, the heating system can track the energy price curves or clean energy output curves without significant effects on the occupants' thermal comfort.

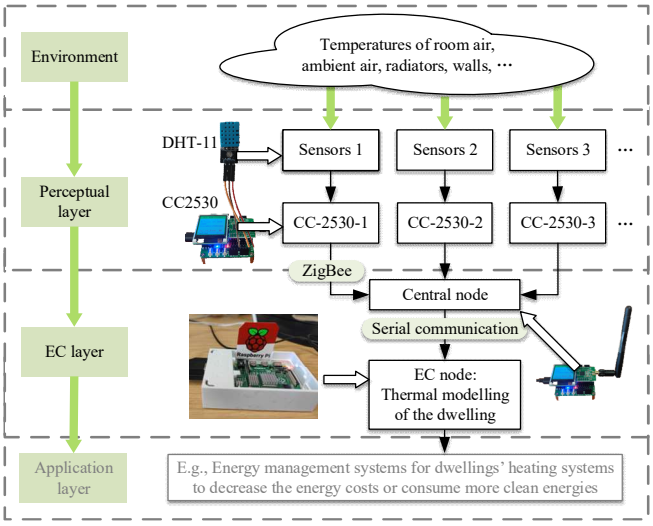

Fig. 1. Architecture of the ZigBee-supported EC system

III. Thermal Model of a Single Room

Since the thermal model for a whole dwelling building can be represented by several typical rooms, this paper focuses on the thermal modelling of separated rooms. The thermal exchange of a single room is presented in Fig. 2. As shown, the air inside the room can store a certain amount of heat, denoted as Q_r, which varies over time and can be calculated by (1).

$$Q_r(t) = c_r \rho_r V_r T_r(t) \quad (1)$$

The change of Q_r is determined by the heat exchange between the room air and ambient air, other rooms and disturbances [27], as shown in (2). Q_{h2r}, Q_{d2r}, Q_{r2a} and Q_{r2w} are the heat flow between the room air and the radiator, disturbances, ambient air and walls connected to adjacent rooms, respectively. The directions of heat flows are assumed to be the same as those in Fig. 2, where heat is from the heating system and disturbances to the room, and then is transferred to ambient air and walls. And the $\dot{q}_r$ represent the time-varying thermal increment and will be introduced later in this section.

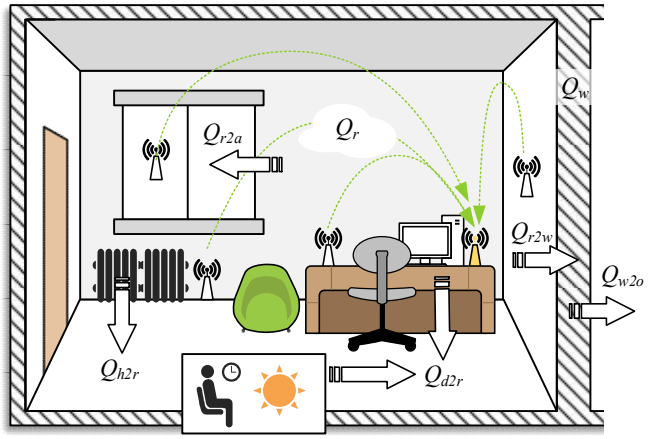

Fig. 2. Thermal exchange and hardware distribution of a single room

$$\frac{dQ_r(t)}{dt} = \dot{Q}_{h2r}(t) - \dot{Q}_{r2a}(t) - \dot{Q}_{r2w}(t) + \dot{Q}_{d2r}(t) + \dot{q}_r(t) \quad (2)$$

The heat flows can be obtained by (3)-(6). The heat from disturbances to room air, Q_{d2r}, is related to many factors, such as the number of occupants, solar radiation, appliance radiation, etc. f_{d2r} is the assumed function of Q_{d2r} to time t, since it is impractical to obtain a physical model of all the disturbances.

$$\dot{Q}_{h2r}(t) = K_{h2r}[T_h(t) - T_r(t)] \quad (3)$$
$$\dot{Q}_{r2a}(t) = K_{r2a}[T_r(t) - T_a(t)] \quad (4)$$
$$\dot{Q}_{r2w}(t) = K_{r2w}[T_r(t) - T_w(t)] \quad (5)$$
$$\dot{Q}_{d2r}(t) = \frac{df_{d2r}(t)}{dt} \quad (6)$$

Obviously, $\dot{Q}_{d2r}$ should be time-varying because its components, such as solar radiation, change over time. Other heat flows also have temporal characteristics. For example, air density in (1) and thermal conductance in (3)-(5) are related to environmental humidity, which varies over time and can be affected by human behaviours and weather conditions.

Therefore, all time-varying components of $\dot{Q}_{h2r}$, $\dot{Q}_{d2r}$, $\dot{Q}_{r2a}$ and $\dot{Q}_{r2w}$ are separated as $\dot{q}_r(t)$ in (2). This makes the heat flows in (2), $\dot{Q}_{h2r}$, $\dot{Q}_{d2r}$, $\dot{Q}_{r2a}$ and $\dot{Q}_{r2w}$, are only determined by constant thermal features, such as thermal conductance and thermal capacity. Since $\dot{q}_r(t)$ and $\dot{Q}_{d2r}(t)$ are unrelated to any state variables, these two are combined as $\dot{Q}'_{d2r}(t)$ to simplify the equation, given by (7).

$$\dot{Q}'_{d2r}(t) = \dot{Q}_{d2r}(t) + \dot{q}_r(t) \quad (7)$$

Based on (1)-(7), the differential equation of room air temperature can be obtained by other temperatures and corresponding coefficients, as (8). Similarly, the temperature differential variation of walls and ambient air can be written as (9) and (10).

$$c_r\rho_r V_r \frac{dT_r(t)}{dt} = -(K_{h2r} + K_{r2a} + K_{r2w})T_r(t) + K_{h2r}T_h(t) + K_{r2a}T_a(t) + K_{r2w}T_w(t) + \dot{Q}'_{d2r}(t) \quad (8)$$

$$c_w m_w \frac{dT_w(t)}{dt} = -(K_{r2w} + K_{w2o})T_w(t) + K_{r2w}T_r(t) + K_{w2o}T_o(t) + \dot{Q}'_{d2w}(t) \quad (9)$$

$$c_a\rho_a V_a \frac{dT_a(t)}{dt} = -(K_{r2a} + K_{a2\varepsilon})T_a(t) + K_{r2a}T_r(t) + K_{a2\varepsilon}T_\varepsilon(t) + \dot{Q}'_{d2a}(t) \quad (10)$$

Based on (8)-(10), a state-space representation of the room thermal model can be written as (11). $\boldsymbol{A}$ and $\boldsymbol{B}$ are the constant feature matrixes of state variables and inputs, respectively. $\boldsymbol{C}$ is the matrix including both constant and time-varying elements. These matrixes enable the interior temperature can be inferred based on weather and radiator conditions. Thus, they are the thermal features that need to be learned by the dark-grey box in the following sections. Since T_o is normally difficult to be obtained (Usually only several typical rooms are measured to evaluate the whole building), it is integrated into $\boldsymbol{C}$. By doing this, all the uncertainties are integrated into matrix $\boldsymbol{C}$ and can be learned by machine learning in the feature learning processes.

$$\begin{bmatrix} \frac{dT_r(t)}{dt} \\ \frac{dT_w(t)}{dt} \\ \frac{dT_a(t)}{dt} \end{bmatrix} = \boldsymbol{A}\begin{bmatrix} T_r(t) \\ T_w(t) \\ T_a(t) \end{bmatrix} + \boldsymbol{B}\begin{bmatrix} T_h(t) \\ T_\varepsilon(t) \end{bmatrix} + \boldsymbol{C} \quad (11)$$

where,

$$\boldsymbol{A} = \begin{bmatrix} \frac{K_{h2r}+K_{r2a}+K_{r2w}}{-c_r\rho_r V_r} & \frac{K_{r2w}}{c_r\rho_r V_r} & \frac{K_{r2a}}{c_r\rho_r V_r} \\ \frac{K_{r2w}}{c_w m_w} & \frac{K_{r2w}+K_{w2o}}{-c_w m_w} & 0 \\ \frac{K_{r2a}}{c_a\rho_a V_a} & 0 & \frac{K_{r2a}+K_{a2\varepsilon}}{-c_a\rho_a V_a} \end{bmatrix},$$

$$\boldsymbol{B} = \begin{bmatrix} \frac{K_{h2r}}{c_r\rho_r V_r} & 0 \\ 0 & 0 \\ 0 & \frac{K_{a2\varepsilon}}{c_a\rho_a V_a} \end{bmatrix}, \text{ and } \boldsymbol{C} = \begin{bmatrix} \frac{\dot{Q}'_{d2r}}{c_r\rho_r V_r} \\ \frac{\dot{Q}'_{d2w}}{c_w m_w} + \frac{K_{r2o}}{c_w m_w}T_o \\ \frac{\dot{Q}'_{d2a}}{c_a\rho_a V_a} \end{bmatrix}$$

When the time step, Δt, is small, the differential equation (11) can be approximately converted to a difference equation, as shown in (12). In this paper, the unit time interval of the thermal model is set as 1 minute. Then, with Δt set as the unit time interval, (13) can be obtained based on (11)-(12).

$$\frac{dT_{r,w,a}(t)}{dt} \approx \frac{T_{r,w,a}(t+\Delta t) - T_{r,w,a}(t)}{\Delta t} \quad (12)$$

$$\begin{bmatrix} T_r(t+1) \\ T_w(t+1) \\ T_a(t+1) \end{bmatrix} \approx (\boldsymbol{A} + \boldsymbol{I})\begin{bmatrix} T_r(t) \\ T_w(t) \\ T_a(t) \end{bmatrix} + \boldsymbol{B}\begin{bmatrix} T_h(t) \\ T_\varepsilon(t) \end{bmatrix} + \boldsymbol{C} \quad (13)$$

where $\boldsymbol{I}$ is a 3×3 identity matrix.

Here, Δt is set as 1 minute, which is small enough compared to the temporal thermal signature of dwellings. Thus, the transformation from (11) to (13) has little impact on the accuracy of the thermal model but can significantly reduce computing complexities in obtaining the numerical solutions for (11). Then, based on (13), the problem is to accurately learn

matrixes $\boldsymbol{A}$, $\boldsymbol{B}$ and $\boldsymbol{C}$ from historical data. Since $\boldsymbol{C}$ contains both constant and time-varying elements, to simplify the following analysis, $\boldsymbol{C}$ is divided into a constant part $\overline{\boldsymbol{C}}$ and a time-varying part $\widetilde{\boldsymbol{C}}(t)$ to be learned by grey box and black box, respectively, as presented in (14).

$$\boldsymbol{C} = \overline{\boldsymbol{C}}_{3\times1} + \widetilde{\boldsymbol{C}}(t)_{3\times1} \tag{14}$$

The current thermal model is limited by the sensor numbers, thus only the temperatures of ambient air, radiator, room air and walls are available. However, with more or fewer sensors, the thermal model in (8)-(11) can be flexibly expanded or contracted. Since the form of (11) will not change (only the dimension of (11) changes), the following procedures of the dark-grey box are still the same.

IV. Development of the Dark-Grey Box

The dark-grey box is developed for thermal modelling of dwellings and consists of two steps: i) a grey box, based on the physical thermal model in (13), learns the constant features by a method pool; ii) a black box, only relying on historical data but a physical model, is applied to learn the time-varying features by deep GRU networks. The diagram of the dark-grey box is presented in Fig. 3.

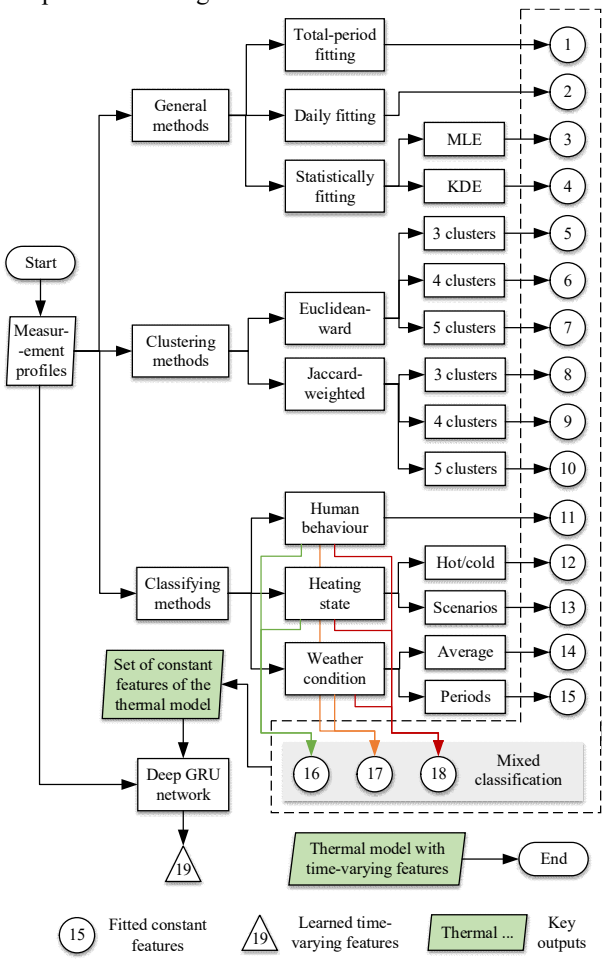

Fig. 3. Dark-grey box for feature learning of dwelling thermal models

For the first step, the grey box, the constant features consist of the coefficients in matrixes $\boldsymbol{A}$, $\boldsymbol{B}$ and $\overline{\boldsymbol{C}}$. The constant features are learned by PSO-based optimisation with different strategies. To obtain the most accurate constant features of the thermal model, many learning strategies are considered as a method pool. Specifically, for constant feature learning, three categories of methods are utilised: general methods, clustering methods and classifying methods, as shown in Fig. 3. Each category includes several learning strategies. These methods show different performances with different historical data sizes in the case study thus it is important to build a method pool to select better learning strategies in real operations. Specifically, with these many methods, the dark-grey box can select the most accurate grey-box model and periodically update it. In this way, the customers can obtain both accurate thermal models and specific timely thermal parameters of their dwelling rooms.

After the constant feature learning, the results are put into a deep GRU network to learn $\widetilde{\boldsymbol{C}}(t)$. The GRU deep neural network can derive the time-sequence regularities, which enables the black box to learn the time-varying features in the room's thermal model. Then, a final room's thermal model is obtained with constant matrixes $\boldsymbol{A}$ and $\boldsymbol{B}$, and $\boldsymbol{C}$. The dark-grey box in the 19th method consists of a grey box to obtain the constant features and a black box to improve its accuracy by learning time-varying features. The grey box provides physical basis for the black box to make it easy to interpret and the black box enhances the accuracy of the grey box.

A. Constant Features Learning in Grey Box

The constant feature learning is developed as a grey box to obtain an accurate set of $\boldsymbol{A}$, $\boldsymbol{B}$ and $\overline{\boldsymbol{C}}$. Some strategies are applied, which can be divided into three categories: general, clustering and classifying, as shown in Fig. 3. Some strategies applied in previous research are combined in the general method set, including total-period learning, daily learning and statistical learning. The above methods in the general set could be simple but lack accuracy. Thus, clustering and classifying methods are considered in the method pool of the grey box.

Clustering methods divided the training set into several clusters, and each of the clusters contains several days that have similar temperature curves. The clustering basis is the correlation and similarity between the days in the training set.

The classifying method also divides the training set into several groups but is based on human or physical knowledge. For example, a room with or without occupants should have different temperature curves for different thermal needs. Therefore, based on human behaviour, heating state and weather condition, the training set is specifically divided into many groups. Each group will be learned separately to achieve a more accurate thermal model in each classified condition.

The following subsections describe the three method sets:

1) General Methods

First, for the general methods, the simplest strategy uses one set of $\boldsymbol{A}$, $\boldsymbol{B}$ and $\overline{\boldsymbol{C}}$ to learn the whole period of the training set. This learning problem can be seen as an optimisation problem to obtain the optimal coefficients in $\boldsymbol{A}$, $\boldsymbol{B}$ and $\overline{\boldsymbol{C}}$. The objective function of this optimisation, f_1, is to minimise the variance between the learned and real temperature of room air, as shown in (15). $\boldsymbol{e}(t)$ is the learning error at t^{th} time slot, calculated by

(16). The reason for using variance rather than absolute error is that a larger learning error leads to a more uncomfortable experience for occupants.

$$f_1 = min \sum_{t=2}^{T_{train}} e_1(t)^2 \tag{15}$$

$$\boldsymbol{e}(t) = \begin{bmatrix} e_1(t) \\ e_2(t) \\ e_3(t) \end{bmatrix} = \begin{bmatrix} T_r(t) \\ T_w(t) \\ T_a(t) \end{bmatrix} - (\boldsymbol{A}' + \boldsymbol{E}) \begin{bmatrix} T_r(t-1) \\ T_w(t-1) \\ T_a(t-1) \end{bmatrix} - \boldsymbol{B}' \begin{bmatrix} T_h(t-1) \\ T_\varepsilon(t-1) \end{bmatrix} - \overline{\boldsymbol{C}}' \tag{16}$$

where T_{train} is the period of the training set, $\boldsymbol{A}'$, $\boldsymbol{B}'$ and $\overline{\boldsymbol{C}}'$ are the constant matrixes learned by the optimisation.

The thermal model utilised in heating system optimisation is usually used for day-ahead planning, where the period of forecasted temperature curves is 24 hours. Therefore, the second strategy aims to use one set of $\boldsymbol{A}$, $\boldsymbol{B}$ and $\overline{\boldsymbol{C}}$ to learn each day separately and obtain the optimal coefficients for $\boldsymbol{A}$, $\boldsymbol{B}$ and $\overline{\boldsymbol{C}}$. The objective function, f_2, is presented in (17).

$$f_2 = min \sum_{d=1}^{N_{day}} \sum_{t=2}^{T_{day}} e_1(t)^2 \tag{17}$$

where T_{day} is a typical day of 1440 minutes, N_{day} is the number of days in the training set.

In the above optimisation, every day shares the same set of constant features. Nevertheless, if each day can be learned by different sets of $\boldsymbol{A}$, $\boldsymbol{B}$ and $\overline{\boldsymbol{C}}$, the learning accuracy could be much higher. The objective function of this strategy $f_{3-4,d}$ is shown in (18) with its learning error in (19).

$$f_{3-4,d} = min \sum_{t=2}^{T_{day}} e_{1,d}(t)^2, d = 1, 2, \dots, N_{day} \tag{18}$$

$$\boldsymbol{e}_d(t) = \begin{bmatrix} e_{1,d}(t) \\ e_{2,d}(t) \\ e_{3,d}(t) \end{bmatrix} = \begin{bmatrix} T_r(t) \\ T_w(t) \\ T_a(t) \end{bmatrix} - (\boldsymbol{A}'_d + \boldsymbol{E}) \begin{bmatrix} T_r(t-1) \\ T_w(t-1) \\ T_a(t-1) \end{bmatrix} - \boldsymbol{B}'_d \begin{bmatrix} T_h(t-1) \\ T_\varepsilon(t-1) \end{bmatrix} - \overline{\boldsymbol{C}}'_d \tag{19}$$

The number of optimal sets of $\boldsymbol{A}$, $\boldsymbol{B}$ and $\overline{\boldsymbol{C}}$ is equal to the days' number in the training set. These results are the optimal learned features for each specific day in the training set but have limited accuracy in the testing set. Therefore, statistical methods, MLE and KDE, are utilised to obtain a rational set of constant features. MLE is to estimate constant features from their probability distributions. However, sometimes the probability distribution of constant features cannot match any of the known probability distribution models. Then, KDE is used as a non-parametric way to estimate the probability density function of the coefficients in $\boldsymbol{A}$, $\boldsymbol{B}$ and $\overline{\boldsymbol{C}}$.

2) Clustering Methods

Two clustering methods are selected in this step: Euclidean-ward and Jaccard-weighted. Euclidean-ward is a widely used clustering method for calculating the minimum variance of Euclidean distance between data points. Days in the training set will be clustered into several groups, where the daily curves of $T_\varepsilon(t)$ are similar to each other. And for the Jaccard-weighted method, the days in the training set are divided according to the Jaccard correlation value of $T_\varepsilon(t)$. The days which have more closely correlated $T_\varepsilon(t)$ are aggregated together as a group to train one set of $\boldsymbol{A}$, $\boldsymbol{B}$ and $\overline{\boldsymbol{C}}$.

The objective function of the two clustering methods, $f_{5-10,l}$, can be written as (20). To explore the impact of clustering numbers on the accuracy of the constant feature learning, we have clustered the train-set into 3, 4 and 5 groups, as shown in Fig. 3. The corresponding error can be calculated by (21).

$$f_{5-10,l} = min \sum_{d=1}^{N_{day,l}} \sum_{t=2}^{T_{day}} e_{1,l}(t)^2 \tag{20}$$

$$\boldsymbol{e}_l(t) = \begin{bmatrix} e_{1,l}(t) \\ e_{2,l}(t) \\ e_{3,l}(t) \end{bmatrix} = \begin{bmatrix} T_r(t) \\ T_w(t) \\ T_a(t) \end{bmatrix} - (\boldsymbol{A}'_l + \boldsymbol{E}) \begin{bmatrix} T_r(t-1) \\ T_w(t-1) \\ T_a(t-1) \end{bmatrix} - \boldsymbol{B}'_l \begin{bmatrix} T_h(t-1) \\ T_\varepsilon(t-1) \end{bmatrix} - \overline{\boldsymbol{C}}'_l \tag{21}$$

where $N_{day,l}$ is the number of days in l^{th} cluster.

3) Classifying Methods

When the size of the training set is small, data features are hard to be accurately derived by clustering methods. Thus, human experience and physical knowledge are considered to classify the training set into several groups. Three factors, which may have huge impacts on dwelling thermal features, are selected: human behaviour, heating state, and weather condition.

For human behaviour, when occupants are inside the room, the room temperature is usually higher and more stable. The objective function, f_{11}, is written as (22). Similar to (19) and (21), errors $e_{1,1}$ and $e_{1,2}$ lead to two different sets of $\boldsymbol{A}$, $\boldsymbol{B}$ and $\overline{\boldsymbol{C}}$, denoted as $\boldsymbol{A}'_1$, $\boldsymbol{B}'_1$, $\overline{\boldsymbol{C}}'_1$ and $\boldsymbol{A}'_2$, $\boldsymbol{B}'_2$, $\overline{\boldsymbol{C}}'_2$ respectively. To present other following classifying methods, (22) can be also presented as (23), where $N_\omega = 2$.

$$f_{11} = \min \left[\sum_{d=1}^{N_{day}} \sum_{t=2}^{T_{day,1}} e_{1,1}(t)^2 + \sum_{d=1}^{N_{day}} \sum_{t=2}^{T_{day,2}} e_{1,2}(t)^2 \right] \tag{22}$$

$$f_{11-13,15-18} = \min \sum_{\omega=1}^{N_\omega} \sum_{d=1}^{N_{day}} \sum_{t=2}^{T_{day,\omega}} e_{1,\omega}(t)^2 \tag{23}$$

where $T_{day,1}$ and $T_{day,2}$ are periods when occupants inside and outside, errors $e_{1,\alpha}$ and $e_{1,\beta}$ are the corresponding learning errors, N_ω is the number of classified groups in one day.

It is also noted that the heat state of radiators and weather temperature also largely alter the temperature features of a room. Fig. 4 presents the classification principle of these two factors. The heating states are defined in two or four categories, as shown in Fig. 4(a). The red and green dash areas represent the high-power and low-power periods, respectively. And these two periods can be further divided into temperature climbing, high-temperature stable, temperature decreasing, and low-temperature stable periods. The Fig. 4(b) shows the period classification of weather temperature, as $< 4℃$, $4-6℃$, $6-8℃$, $8-10℃$ and $> 10℃$.

As shown in Fig. 4(a), with the heating state converted from high to low power, the room's temperature will first rapidly decrease and then converge to a certain value. In this condition, the heat capacity of room air could be different from other conditions because of the higher humidity. Therefore, based on

different heating states: high-temperature level and low-temperature level, the days can be divided into two conditions, with the same objective function in (23) and $N_\omega = 2$. In this condition, $e_{1,1}$ and $e_{1,2}$ refers to the error of high-power periods and low-power periods.

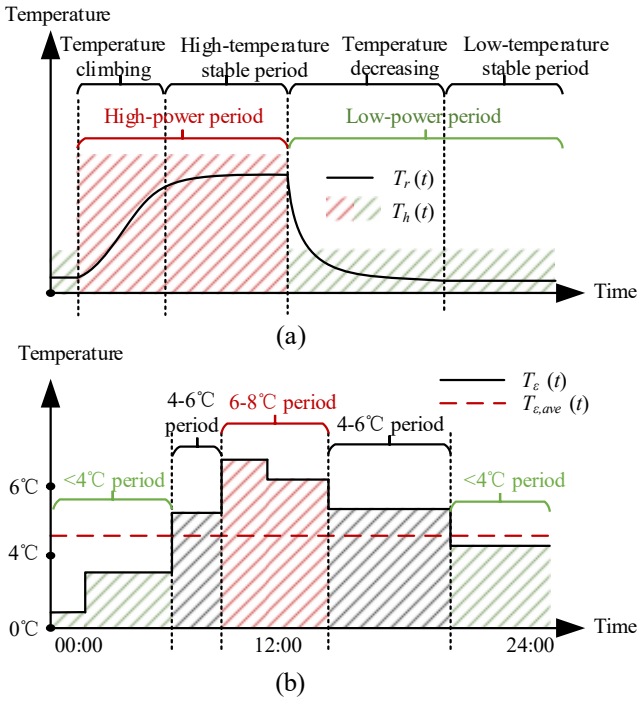

Fig. 4. Diagram of periods classification according to heating states (a) and weather conditions (b)

In addition, the heating state can be further divided into 4 scenarios as shown in Fig 4 (a). The two stable periods are the same as the high and low-temperature periods above. And the temperature climbing and decreasing periods are separated from the training set to learn if there are any different thermal features when the temperature is drastically changing. For example, the thermal conductance between the heating radiator and room air is proved to be higher when the temperature climbs fast. In this way, there are four scenarios in this method, as $N_\omega = 4$ in (23), which leads to 4 sets of $\boldsymbol{A}$, $\boldsymbol{B}$ and $\overline{\boldsymbol{C}}$.

Weather condition is considered as the third classification basis. When the temperature is low with strong wind, the thermal conductance between room air and ambient air is higher than usual. When the temperature is mild with little wind, the value could be lower. Therefore, we have divided the weather by two strategies: 1) the average temperature of a whole day and 2) temperature-range periods inside one day.

For the first one, the days in the training set are classified into five groups according to their average temperature, as shown in Fig. 4(b). The red dotted line is the average temperature of this day, $T_{\varepsilon,ave}$, and belongs to the $4-6$℃ group. The objective function of this strategy is shown in (24), where $N_{day,tem}$ is the number of days in a group with a certain temperature range, and $e_{1,tem}$ is the learning error of the tem^{th} group.

$$f_{14,tem} = min \sum_{d=1}^{N_{day,tem}} \sum_{t=2}^{T_{day}} e_{1,tem}(t)^2 \quad (24)$$

The second strategy classifies temperature periods within each day, as the green, grey and red dash areas shown in Fig. 4 (b). A day is divided into several periods according to the variations in weather temperature. The periods within the same temperature ranges in the training set will be learned together. This strategy has the same objective function as (23) with $N_\omega = 5$, for the five weather temperature ranges.

Finally, as shown in Fig. 3, to further classify the training set, the three classifying bases are mixed into three more classifications: Holiday-Heating, Holiday-Weather, and Holiday-Heating-Weather. The hot/cold state of radiators and weather periods strategies are utilised. Thus, the value of N_ω of the three mixed classifications are 2×2, 2×5 and 2×2×5. And the objective function is the same as $f_{11-13,15-18}$ in (23), only with different group numbers in a day.

Then, with the general, clustering and classifying methods, a total number of 18 learning results (as shown in No.1-18 in Fig. 3) of constant features is obtained in the grey box as the constant feature set. All learning results will be taken as input for the time-varying feature learning in the black box.

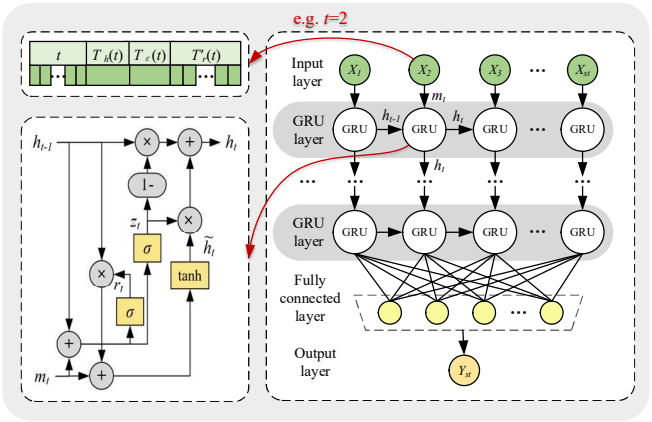

Fig. 5. Deep GRU network for time-varying feature learning

B. Time-Varying Features Learning in Black Box

A deep GRU network is applied to learn the time-varying features ($\widetilde{\boldsymbol{C}}$ in (14)) of dwelling thermal models. The reasons for utilising GRU are 1) GRU network is efficient for time-sequence learning without serious gradient vanishing and exploding problems [25]. 2) The learning curve of GRU has hysteresis quality [28]. This is suitable for thermal model learning because the room temperature follows the alternation of radiators and weather conditions. 3) Curves learned by GRU tend to be very smooth and room temperature changes usually slowly and smoothly.

The deep GRU network is composed of the input layer, several GRU layers, a fully connected layer and an output layer. As shown in the upper left part of Fig. 5. The inputs include 1) temporal information, such as date, hour, minute, week and holiday; 2) expected temperature of the radiator and local weather, as $T_h(t)$ and $T_\varepsilon(t)$.; 3) learning results from grey boxes, as $T'_r(t)$. X_{st} and Y_{st} are the inputs and outputs at the maximum time step.

The inputs are sent to the multilevel GRU layer, which contains many GRU cells, as illustrated in the left side of Fig.

5. m_t is the time-sequence input of a GRU cell, and h_t is its output, calculated by (25). z_t and r_t are the update gate and reset gate of the GRU cell, which are the key procedures in GRU cells and can be formulated as (26)-(27). The weight vectors of the two gates $\boldsymbol{W}_z$ and $\boldsymbol{W}_r$ are trained based on the sigmoid function σ. $\tilde{h}_t$ denotes the candidate's hidden state of the GRU cells, shown as (28).

$$h_t = (1 - z_t) \times h_{t-1} + z_t \times \tilde{h}_t \tag{25}$$

$$z_t = \sigma\left[\boldsymbol{W}_z \cdot [h_{t-1}, m_t]\right] \tag{26}$$

$$r_t = \sigma\left[\boldsymbol{W}_r \cdot [h_{t-1}, m_t]\right] \tag{27}$$

$$\tilde{h}_t = \tanh\left[\boldsymbol{W}_h \cdot [r_t \times h_{t-1}, m_t]\right] \tag{28}$$

After the learning of the deep GRU network, a new learning result of $\tilde{T}_r(t)$, $\tilde{T}_w(t)$ and $\tilde{T}_a(t)$ will be obtained. Based on these new outputs, the time-varying features can be calculated by (29). With the value of $\widetilde{\boldsymbol{C}}$, the temporal influence on temperature alternations can be revealed and makes the results of the black box easier to be interpreted based on the physical model in (29).

$$\widetilde{\boldsymbol{C}}(t) = \begin{bmatrix} \tilde{T}_r(t) \\ \tilde{T}_w(t) \\ \tilde{T}_a(t) \end{bmatrix} - (\boldsymbol{A}_l' + \boldsymbol{E}) \begin{bmatrix} T_r(t-1) \\ T_w(t-1) \\ T_a(t-1) \end{bmatrix} - \boldsymbol{B}_l' \begin{bmatrix} T_h(t-1) \\ T_\varepsilon(t-1) \end{bmatrix} - \overline{\boldsymbol{C}}_l' \tag{29}$$

V. Case Study

The proposed 2-stage dark-grey box is demonstrated based on the real data collected from a university office. Similar to the hardware layout diagram in Section III, as presented in Fig. 6, the sensors are deployed at the outside window, heating radiator, room inside and walls connected to other rooms. The CC2530 board is utilised as the communication module between end-side sensors and the EC node. DHT11 is applied in this case as the temperature sensor. Temperature data are collected from 20/11/2021 to 29/01/2022, including 70 days. The measured curves are presented in Fig. 7 with the real weather data [29].

As shown in Fig. 7, the room air temperature keeps changing following the change of heating state and weather conditions. Besides, this period contains the Christmas holiday. This provides various scenarios for the dark-grey box of the dwelling thermal model, including different heating states, weather conditions and human behaviours. The high-power periods in Fig. 4 (a) are the periods that have average temperatures over 35 °C, and the rest of the time is low-power periods. The temperature climbing and decreasing periods are set as the 4-hour periods between the high and low power periods. This is because normally the temperature of room air is stable after 4 hours from the alternation of the heating state.

Firstly, the data collected in 50 days is taken as the training set, with the data collected in the other 20 days as the testing set. The training set is randomly selected and repeated 10 times. The learning accuracy error of the developed dark-grey box is shown in Table I, where MAE, MSE and MAPE refer to Mean Absolute Error, Mean Squared Error and Mean Absolute Percentage Error. The optimisation method utilised in constant features is PSO and the optimisation for each training set is repeated 10 times. The errors in Table I are the average values of the simulation result from each method in Fig. 3.

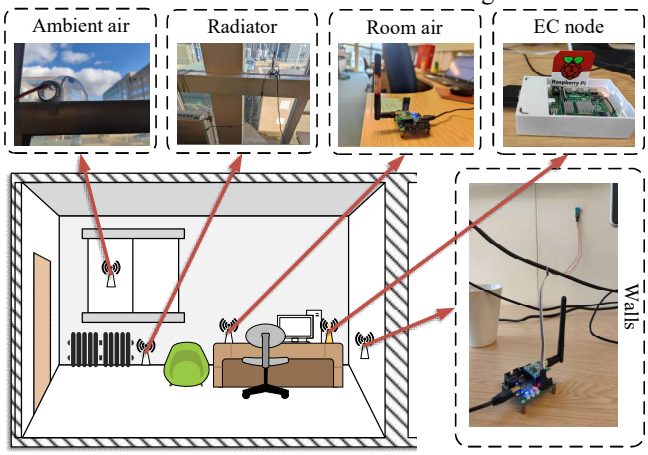

Fig. 6. Hardware distribution of the demonstrated case

As shown in Table I, shallow green, yellow and red grids are the most, second and third accurate results in each condition, respectively. The method numbers can be found in Fig. 3. The classifying methods perform better than others in both the training set and testing set, especially the mixed classification strategies. In the testing set, the classification based on human behaviours and weather conditions is the most accurate strategy, with 93.2% accuracy and 1.43 °C absolute error. The result of the deep GRU network is even better. With the constant learning results, the GRU method can increase the accuracy to 94.2% with 1.15 °C absolute error. The MAPE is decreased by 14.7% compared with the best constant feature learning results. In this condition, the error is decreased to nearly 1 °C, which makes the temperature scheduled by heating controllers based on this dark-grey box more comfortable to the occupants.

The learning results of two days in the testing set are in Fig. 8. This two-day period contains temperature climbing and decreasing conditions and has a certain time length of high-power and low-power periods. As shown in Fig. 8, the GRU method is more capable of capturing the temperature increases during middays and afternoons. This means time-varying features have a comparatively large value at noon. And sometimes, time-varying features have negative values at night.

Besides the GRU method, the most accurate methods are the classifying method, especially the one classified by weather and human behaviour, denoted as the 17th method in Fig. 3. This can be observed from the third accurate result in Table I, where the 17th method produces better results among non-GRU methods. The well-learned constant feature of this method is presented in Table II. Since the thermal conductance of walls is usually much higher than air, $c_w m_w$ is comparatively huge. The result of $(\frac{\dot{Q}'_{d2w}}{c_w m_w} + \frac{K_{r2o}}{c_w m_w} T_o)$ shows that the other rooms' impact on the testing room is small. In addition, the value of $K_{a2\varepsilon}$ is small, which means the measured weather temperature is very close to the data given by the weather station. These well-learned thermal features produce valuable information to customers. This also indicates the advantages of grey boxes over black ones: accurate and easy to interpret.

It is worth mentioning that the accuracy of the deep GRU network highly relies on the data size of the training set. The learning results in Table III present the performances of all the methods with different train sizes. The shallow green, yellow and red grids are the most, second and third accurate results in each condition, respectively. When the data size is huge and more than one month's data can be learned, the GRU and classifying methods are the better choices. The accuracy of GRU is always higher than 93%.

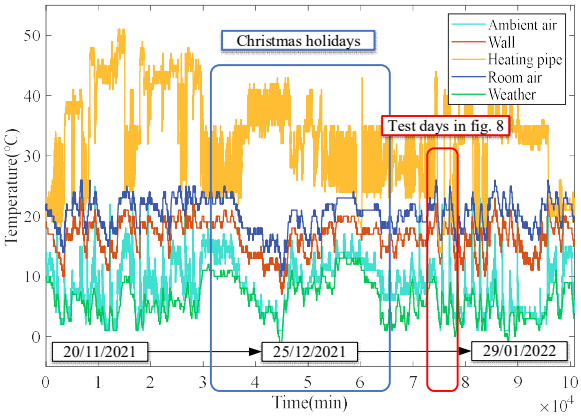

Fig. 7. Measured temperatures and real weather data of Bath, UK, from 20/11/2021 to 29/01/2022

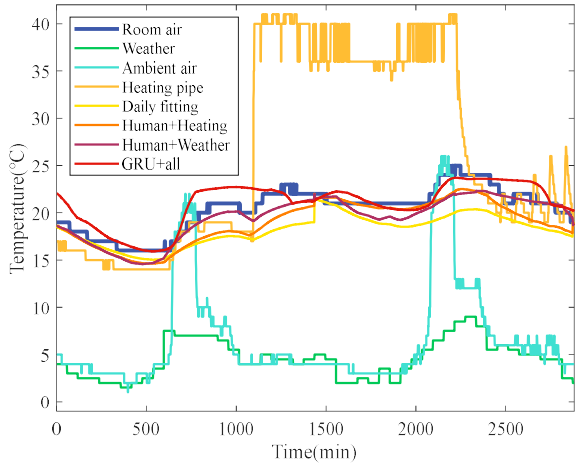

Fig. 8. Learning results, measured temperatures and real weather data of Bath, UK, on 12/01/2021 and 13/01/2022

A. Dark-grey box with limited data size

In real operation, the train data size could be really small, maybe even less than two weeks. In this condition, the data-size-dependent methods perform worse, with an error rate increase to 12.3% when only 10 days can be trained. However, the classifying method based on human behaviours and heating states still maintains a high accuracy of around 92% when the training size is 30 or 20 days. Besides, the clustering methods could be more accurate in this condition, especially the Jaccard-weighted method which becomes the second-best method when the training set is less than 30 days.

TABLE I
LEARNING RESULTS OF ALL METHODS WITH 50 DAYS AS THE TRAINING SET

Method number	Training set			Testing set		
	MAE (℃)	MSE	MAPE (%)	MAE (℃)	MSE	MAPE (%)
1	1.67	4.70	8.93	1.75	4.91	8.18
2	1.54	3.95	8.09	1.95	6.11	9.02
3	3.29	14.8	15.5	4.29	22.5	20.2
4	9.21	94.2	44.4	9.79	99.8	47.0
5	1.43	3.59	7.51	1.64	4.65	7.58
6	1.38	3.57	7.27	1.67	4.76	7.86
7	1.35	3.56	7.21	1.68	4.89	7.86
8	1.47	3.83	7.79	1.60	4.60	7.39
9	1.42	3.71	7.58	1.69	4.91	7.78
10	1.39	3.53	7.34	1.60	4.19	7.48
11	1.45	3.52	7.60	1.87	6.03	8.75
12	1.49	3.71	7.83	1.81	5.70	8.41
13	1.31	3.29	6.91	1.66	4.79	7.75
14	1.39	3.34	7.15	1.92	6.19	8.92
15	1.25	2.69	6.54	1.44	3.23	6.93
16	1.08	2.11	5.63	1.44	3.54	6.92
17	1.13	2.24	5.84	1.43	3.35	6.81
18	1.07	2.17	5.51	1.67	4.34	8.22
19				1.15	2.36	5.82

TABLE II
WELL-LEARNED CONSTANT THERMAL FEATURES

Thermal capacity	$c_r\rho_r V_r$	$c_w m_w$			$c_a\rho_a V_a$
Learned value	30.39	$9.4*10^5$			0.62
Thermal conductance	K_{h2r}	K_{r2a}	K_{r2w}	K_{w2o}	$K_{a2\varepsilon}$
Learned value	0.031	0.25	$6.4*10^{-3}$	8.1	0.093
Constant part in $\boldsymbol{C}$	$\frac{\dot{Q}'_{d2r}}{c_r\rho_r V_r}$	$\frac{\dot{Q}'_{d2w}}{c_w m_w}+\frac{K_{r2o}}{c_w m_w}T_o$			$\frac{\dot{Q}'_{d2a}}{c_a\rho_a V_a}$
Learned value	0.022	$9.21*10^{-5}$			0.064

TABLE III
LEARNING MAPE (%) OF ALL METHODS WITH DIFFERENT TRAINING SET SIZE

Method number	60 days	50 days	40 days	30 days	20 days	10 days
1	8.19	8.18	9.79	9.84	10.3	9.78
2	8.47	9.02	10.0	10.1	7.74	9.49
3						
4						
5	7.53	7.58	13.2	10.1	7.89	10.0
6	7.62	7.86	11.8	10.6	10.6	18.5
7	7.29	7.86	11.5	10.0	9.56	16.1
8	7.15	7.39	11.1	9.76	8.25	10.1
9	7.97	7.78	11.3	10.2	8.24	9.32
10	7.14	7.48	9.62	9.48	8.01	9.28
11	9.09	8.75	12.3	11.9	9.87	9.54
12	8.24	8.41	10.3	12.4	9.61	9.41
13	7.03	7.75	12.3	10.9	9.64	13.4
14	8.81	8.92	11.2	10.4	8.13	10.1
15	7.11	6.93	9.91	8.03	8.71	9.50
16	7.45	6.92	7.88	7.76	7.34	9.22
17	6.73	6.81	9.26	10.7	9.46	11.4
18	6.59	8.22	7.78	8.34	8.76	16.8
19	5.68	5.82	6.92	8.42	10.1	12.3

In addition, as shown in Table III, the gap between the accuracy of 60 days and 50 days is comparatively small. This gap will be much less with the growth of data size. This is because when the data is far from now, the weather and dwelling condition has already changed, which makes it less meaningful to the current thermal model.

The case study justifies that the dark-grey box with well-learned time-varying features can accurately learn the thermal model of dwellings with a comparatively large dataset. Specifically, the MAPE of the dark-grey box is decreased by 14.7% compared with the best results of grey boxes. When the size of the dataset is small, the clustering and classifying

methods developed in this paper have better performance. This could provide valuable information in real operations to avoid data dependency on machine learning.

B. Dark-grey box with limited sensors

Since temperature measurements could be incomplete in practice, the developed dark-grey box is tested with different measurements, as presented in Table IV. The two state variables, the temperature of walls and ambient air are assumed to be unavailable separately and both, as Without T_w, Without T_w, Without T_a and T_w, in Table IV (taking 50 days as the training set). In this condition, the dimension of the state matrix in (11) will be decreased. The results show that without T_a or T_w, the accuracy of the dark-grey box is decreased, and T_a could be more influential to the dark-grey box. The temperatures of the weather and radiator are core inputs for thermal models. Thus, if these measurements are unavailable, the thermal model is altered to a total black box. As shown in Table IV, assuming only T_r is accessible, the black box has significant inaccuracy compared to the dark-grey box.

TABLE IV
RESULT COMPARISON OF THE DARK-GREY BOX WITH DIFFERENT MEASUREMENTS

Measurements	All	Without T_w	Without T_a	Without T_a and T_w	Only T_r
MAPE (%)	5.68	6.43	6.71	7.15	8.16

C. Comparison with non-machine-learning methods

In this paper, all the methods are based on machine learning, because, i) there are many unknown parameters in the thermal model, ii) the time sequence of the training set is long, and iii) machine-learning methods can provide an effective solution for a problem like this and have been utilised in many studies [8, 22-24]. Although, as a comparison, a nonlinear regression method based on least square fitting is demonstrated. The result of this method shows that, with appropriate initial values, MAPE values of the testing and training set are around 9% and 12%, respectively (taking 50 days as the training set). This is much higher than the machine learning methods utilised in the dark-grey box. Besides, sometimes, the method cannot converge with different initial values. Comparatively, in the developed dark-grey box, the initial values can be randomly selected, and the method always converges, which brings significant advantages in real operations.

VI. OUTLOOK

The IoT platform and the dark-grey box in this work are mainly developed to provide an accurate thermal model based on machine learning methods. This thermal model can be utilised in many scenarios in real operations:

- Smart homes: The smart control of heating systems is core for smart homes. To intelligently maintain the interior temperature within a comfortable range, an accurate thermal model to infer the change of temperature is necessary.
- Energy management systems: Based on an accurate thermal model, the change of interior temperature caused by operations of EMS can be rationally estimated. Thus, the optimisation of energy management can be more effective.
- Decarbonisation: Residential energy systems play an important role in decarbonisation. With an accurate thermal model, the energy consumed by heating systems can be scheduled to follow clean energy resources.

Temperature is the only physical information for this developed platform. With more sensors, air humidity, human motions, electricity and water consumption, etc., can all be monitored. Besides, household appliances, energy storage systems and residential renewable energy systems can be centrally controlled by this platform via suitable communication methods, such as ZigBee. In this way, more intelligent functions can be realised with this platform. Therefore, the future investigation of this platform and dark-grey box could mainly focus on practical applications to enable more smart operations of energy systems.

VII. CONCLUSION

This paper develops a dark-grey box to learn dwelling thermal models based on edge computing. A ZigBee-based edge computing platform is utilised as the hardware platform. This platform is easy to operate and can be used for long-term time. A thermal model with time-varying features is developed. A method pool, including general, clustering, classifying and machine learning methods, is applied to the dark grey box to learn features of dwelling thermal models. The case study illustrates the dark-grey box with well-learned time-varying features can accurately learn the thermal model of dwellings. Specifically, the MAPE of the dark-grey box decreases significantly compared with the best results of grey boxes. When the dataset size is small, the developed clustering and classifying methods have even better performance. This work provides a more accurate thermal modelling approach and can produce insights in real operations to avoid data dependency on machine learning. Without better modelling, the work can enable more efficient energy use and management, thus helping reduce energy costs for heating.

REFERENCE

[1] "Energy consumption and use by households " in "Products Eurostat News," Eurostat, European Commission, 2020. [Online]. Available: https://ec.europa.eu/eurostat/web/products-eurostat-news/-/ddn-20200626-1

[2] "ECUK 2021: Consumption data tables (Excel)," 2022. [Online]. Available: https://assets.publishing.service.gov.uk/government/uploads/system/uploads/attachment_data/file/1061634/2021_Consumption_tables_March_2022_update.xlsx

[3] "What's energy used for?," 2015. [Online]. Available: http://www.energyenvoys.org.uk/sites/default/files/What%27s%20energy%20used%20for_0.pdf

[4] S. Bellocchi, M. Manno, M. Noussan, M. G. Prina, and M. Vellini, "Electrification of transport and residential heating sectors in support of renewable penetration: Scenarios for the Italian energy system," Energy, vol. 196, p. 117062, 2020.

[5] H. Saberi, C. Zhang, and Z. Y. Dong, "Data-driven distributionally robust hierarchical coordination for home energy management," IEEE Transactions on Smart Grid, vol. 12, no. 5, pp. 4090-4101, 2021.

[6] L. Yu, T. Jiang, and Y. Zou, "Online energy management for a sustainable smart home with an HVAC load and random occupancy," IEEE Transactions on Smart Grid, vol. 10, no. 2, pp. 1646-1659, 2017.

[7] A. Baniasadi, D. Habibi, O. Bass, and M. A. Masoum, "Optimal real-time residential thermal energy management for peak-load shifting with experimental verification," IEEE Transactions on Smart Grid, vol. 10, no. 5, pp. 5587-5599, 2018.
[8] C. Zagoni. "Data-Driven Thermal Models for Buildings." https://medium.com/analytics-vidhya/data-driven-thermal-models-for-buildings-15385f744fc5 (accessed.
[9] H. Chen, X. Wang, Z. Li, W. Chen, and Y. Cai, "Distributed sensing and cooperative estimation/detection of ubiquitous power internet of things," Protection and Control of Modern Power Systems, vol. 4, no. 1, pp. 1-8, 2019.
[10] W. Shi, J. Cao, Q. Zhang, Y. Li, and L. Xu, "Edge computing: Vision and challenges," IEEE Internet of Things Journal, vol. 3, no. 5, pp. 637-646, 2016.
[11] M. Satyanarayanan, "The emergence of edge computing," Computer, vol. 50, no. 1, pp. 30-39, 2017.
[12] J. Chandramohan, R. Nagarajan, K. Satheeshkumar, N. Ajithkumar, P. Gopinath, and S. Ranjithkumar, "Intelligent smart home automation and security system using Arduino and Wi-fi," International Journal of Engineering And Computer Science (IJECS), vol. 6, no. 3, pp. 20694-20698, 2017.
[13] R. Ramlee, D. Tang, and M. Ismail, "Smart home system for disabled people via wireless bluetooth," in 2012 International Conference on System Engineering and Technology (ICSET), 2012: IEEE, pp. 1-4.
[14] T. Adiono, M. Y. Fathany, S. Fuada, I. G. Purwanda, and S. F. Anindya, "A portable node of humidity and temperature sensor for indoor environment monitoring," in 2018 3rd International Conference on Intelligent Green Building and Smart Grid (IGBSG), 2018: IEEE, pp. 1-5.
[15] S. J. Danbatta and A. Varol, "Comparison of Zigbee, Z-Wave, Wi-Fi, and bluetooth wireless technologies used in home automation," in 2019 7th International Symposium on Digital Forensics and Security (ISDFS), 2019: IEEE, pp. 1-5.
[16] M. Jradi, C. Veje, and B. N. Jørgensen, "A dynamic energy performance-driven approach for assessment of buildings energy Renovation—Danish case studies," Energy and Buildings, vol. 158, pp. 62-76, 2018.
[17] M. Jradi, F. C. Sangogboye, C. G. Mattera, M. B. Kjærgaard, C. Veje, and B. N. Jørgensen, "A world class energy efficient university building by danish 2020 standards," Energy Procedia, vol. 132, pp. 21-26, 2017.
[18] K. Arendt, M. Jradi, H. R. Shaker, and C. Veje, "Comparative analysis of white-, gray-and black-box models for thermal simulation of indoor environment: Teaching building case study," in Proceedings of the 2018 Building Performance Modeling Conference and SimBuild co-organized by ASHRAE and IBPSA-USA, Chicago, IL, USA, 2018, pp. 26-28.
[19] N. Attoue, I. Shahrour, and R. Younes, "Smart building: Use of the artificial neural network approach for indoor temperature forecasting," Energies, vol. 11, no. 2, p. 395, 2018.
[20] T. Lu and M. Viljanen, "Prediction of indoor temperature and relative humidity using neural network models: model comparison," Neural Computing and Applications, vol. 18, no. 4, pp. 345-357, 2009.
[21] M. Macas et al., "The role of data sample size and dimensionality in neural network based forecasting of building heating related variables," Energy and Buildings, vol. 111, pp. 299-310, 2016.
[22] M. Hu, F. Xiao, and L. Wang, "Investigation of demand response potentials of residential air conditioners in smart grids using grey-box room thermal model," Applied energy, vol. 207, pp. 324-335, 2017.
[23] P. Bacher and H. Madsen, "Identifying suitable models for the heat dynamics of buildings," Energy and Buildings, vol. 43, no. 7, pp. 1511-1522, 2011.
[24] G. Bauwens and S. Roels, "Characterizing thermal performance of buildings using dynamic model identification," in Proceedings of the Thermal Performance of the Exterior Envelopes of Whole Buildings XII International Conference, ASHRAE, 2013, pp. 1-14.
[25] J. Chung, C. Gulcehre, K. Cho, and Y. Bengio, "Gated feedback recurrent neural networks," in International conference on machine learning, 2015: PMLR, pp. 2067-2075.
[26] C. Kim, "Measuring power consumption of CC2530 with Z-Stack," Application Note AN079, 2012.
[27] C. Bhamornsiri, "Investigation of the dynamic behavior of heat pumps for the future integration in load management strategies," Power Systems Laboratory, ETH Zürich, Switzerland, 2011.
[28] D. Wei, "Prediction of stock price based on LSTM neural network," in 2019 International Conference on Artificial Intelligence and Advanced Manufacturing (AIAM), 2019: IEEE, pp. 544-547.
[29] "Past Weather in Bath, England, United Kingdom." https://www.timeanddate.com/weather/uk/bath/historic (accessed.

Junlong Li received the B.Eng. degree in the College of Electrical Engineering, Sichuan University, Chengdu, China, in 2019. He is currently pursuing a Ph.D. degree in electronic and electrical engineering at the University of Bath, UK. His main research interests include edge-cloud computing in power systems, EMS and energy system economics.

Chenghong Gu received a Bachelor's degree from the Shanghai University of Electric Power, Shanghai, China, in 2003, and Master's degree from the Shanghai Jiao Tong University, Shanghai, China, in 2007, both in electrical engineering. He received PhD degree from the University of Bath, U.K. He is currently a Reader with the Department of Electronic and Electrical Engineering, University of Bath. His major research interest is in multi-vector energy systems, resilience, and power economics.

Xiangyu Wei received the B.Eng. and B.S. degree in College of Electrical Engineering from Sichuan University, Chengdu, China, in 2019 and 2023. He is currently pursuing the PhD degree in the Department of Electrical and Computer Engineering, the University of Macau, Macao, China. His research interests include forecasting, dispatching and operation of clean energy.

Yue Xiang (Senior Member, IEEE) received the B.S. degree in electrical engineering and automation and the Ph.D. from Sichuan University, Chengdu, China, in 2010 and 2016, respectively. He was a Joint Ph.D. Student with University of Tennessee, Knoxville, TN, USA, from 2013 to 2014. He was a Visiting Scholar with University of Bath, Bath, U.K., in 2015, and a Visiting Researcher with Imperial College London, London, U.K., from 2019 to 2020. He is currently an Associate Professor at Sichuan University. His main research interests include network planning and optimal operation, electric vehicle integration.

Ignacio Hernando-Gil (S'10–M'14) received the Ph.D. degree in power systems from the University of Edinburgh, U.K., in 2014. He is currently Associate Professor at ESTIA Institute of Technology, France, and was previously Prize Fellow at the University of Bath, U.K., and Research Fellow at the University of Edinburgh, U.K. He has research in risk modelling and analysis of active distribution networks and the aggregate impact of smart grid technologies on the quality of power supply.